Flow Cytometric Analysis and Modeling of Cell–Cell Adhesive Interactions: The Neutrophil As a Model

Scott I. Simon, J. David Chambers,* and Larry A. Sklar

Department of Pathology, University of New Mexico, Albuquerque, New Mexico 87131; and *La Jolla Institute for Experimental Medicine, La Jolla, California 92037

Abstract. The immune function of granulocytes, monocytes, lymphocytes, and other specialized cells depends upon intercellular adhesion. In many cases the molecules mediating leukocyte cell adhesion belong to the Leu-CAM superfamily of adhesive molecules. To elucidate the events of homotypic aggregation in a quantitative fashion, we have examined the aggregation of neutrophils stimulated with formyl peptides, where aggregate formation is a transient reversible cell function. We have mathematically modeled the kinetics of aggregation using a linear model based on particle geometry and rates of aggregate formation and breakup. The time course was modeled as a three-phase process, each phase with distinct rate constants. Aggregate formation was measured on the flow cytometer; singlets and larger particles were distinguished using the intravital stain LDS-751. Aggregation proceeded rapidly after stimulation with formyl peptide (CHO-nle-leu-phe-nle-tyr-lys). The first phase lasted 30–60 s; this was modeled with the largest aggregation rate and smallest rate of disaggregation. Aggregate formation plateaued during the second phase which lasted up to 2.5 min. This phase was modeled with an aggregation rate nearly an order of magnitude less than that of the initial fast phase, whereas the disaggregation rate for this phase did not change significantly. A third phase where disaggregation predominated, lasted the remaining 2–3 min and was modeled with a four to fivefold increase of the disaggregation rate. The mechanism of cell–cell adhesion in the plateau phase was probed with the monoclonal antibody IB4 to the CD18 subunit of the adhesive receptor CR3. Based on these studies it appears that new aggregates do not form to a large degree after the first phase of aggregate formation is complete. However, new adhesive contact sites may form within the contact region of these adherent cells to keep the aggregates together.

CELL–cell contact is essential in mediating a variety of cellular and developmental functions. In the immune system, adhesion of leukocytes to adjacent cells is common to lymphocytes, monocytes, macrophages, and granulocytes. These cells are found predominantly as singlets in the resting state in the circulation and respond to a variety of soluble stimuli by forming homotypic aggregates with each other or heterotypic interactions with other cell types. Lymphocyte activation, induction to proliferate, and cytotoxic T-cell binding to target cells are all receptor mediated following intercellular contact (for review see Kuypers and Roos, 1989). The leukocyte family of adhesive molecules designated as Leu-CAM are heterodimeric molecules consisting of a unique alpha subunit (identified as CD11a, CD11b, and CD11c). These are noncovalently bound to a common beta subunit identified as CD18, a 95-kD glycoprotein. Although the molecular structures involved in adhesion of various cell types have been elucidated (for review see Patarroyo and Makgoba, 1989) the mechanism by which these receptors mediate cell–cell contact still needs to be defined.

Homotypic aggregation of neutrophils has been shown to depend upon activation of the complement receptor type 3 (CR3) (Arnout et al., 1985). Neutrophil aggregation in response to a variety of stimuli is blocked in a dose-dependent fashion with MoAB 60.3 to the CD18 epitope (Schwartz et al., 1985). Antibodies that bind to CD11b (alpha) or CD18 (common beta) subunits of CR3 in addition have an inhibitory effect on granulocyte migration (Dana et al., 1986), phagocytosis of unopsonized particles (Klebanoff et al., 1985), and neutrophil-mediated endothelial cell injury (Diener et al., 1985). Neutrophil accumulation in the vasculature and migration to the site of tissue insult may be mediated in part by cell–cell adhesion contributed by CR3 (Bowen et al., 1982; Luscinkas et al., 1989). Neutrophils are the most numerous of the while blood cells and when stimulated to aggregate intravascularly can contribute in a fundamental way to inflammation and ischemic syndromes which result in tissue injury (Jacob and Hammerschmidt, 1981).

Chemotactic peptide stimulation of neutrophils induces transient aggregation both in vivo (Schmid-Schoenbein et

al., 1987), and in stirred cell suspensions (Yuli and Snyderman, 1984; Sklar et al., 1985). Many studies have shown that neutrophil aggregation in response to formyl peptide stimulation depends upon the type of stimulus, the cell density, and the level of degranulation. The kinetics of the aggregation/disaggregation time course is dependent upon the dose and duration of the stimulation. Our studies show the extent of aggregation to be nonlinear; i.e., doubling the cell concentration above the normal physiological range of cells/ml more than doubles the extent of aggregation, particularly increasing the number of large, but nonetheless reversible, aggregates. Reversible aggregation implies that the biochemical events that lead to aggregation are transient or reversible. We observed previously that several other transient cell responses, (O_2^-, actin polymerization, and cell shape change) and a cell signal (Ca^{++}) depend upon new receptor occupancy (Sklar et al., 1985). These responses decay rapidly when receptor binding is inhibited.

Until now, light transmittance as measured by aggregometry has been the primary method of quantitating aggregation. Whereas aggregometry provides a gross measure of the increase in larger aggregates, flow cytometry may be used to analyze the precise size, time course, and distribution of particle size (Sklar et al., 1985). We have developed methodology that enables delineation of particles ranging from singlets and doublets up to quintets on the flow cytometer using a new vital stain LDS-751 (Terstappen et al., 1988). A good correlation has been found between aggregate geometry as measured on the light microscope and the flow cytometer (Rochon, Y. P., and M. Frojmovic, manuscript in preparation).

To define the quantitative aspects of aggregation we have developed a linear aggregation model describing the kinetics of cell interaction. The shifting of the prestimulation equilibrium from singlets to doublets and larger aggregates follows first order kinetics, with the interaction of all particles defined by aggregation and disaggregation rate constants. These rate constants are obtained by analysis of experimental observations of the kinetics of aggregate formation and breakup. By using the flow cytometric techniques, we can characterize these reactions with respect to aggregate size, lifetime, and rates of formation and breakup. A number of publications describing reversible and irreversible models of linear aggregation in other cell types have already appeared (Chang and Robertson, 1976; Bell, 1978, 1981; Capo et al., 1982). However, none of the current studies have quantitatively analyzed the kinetics of neutrophil aggregation in terms of the effect of cell concentration, duration of cell activation, or the mechanism of aggregation at the level of the adhesive receptors.

Materials and Methods

Neutrophils

Human neutrophils were purified from fresh blood by the elutriation procedure which yielded cells of >95% purity (Tolley et al., 1987). Cells were washed in a modified Geys buffer (10 mM KCl, 110 mM NaCl, 10 mM glucose, 1 mM $MgCl_2$, and 30 mM Hepes, pH 7.45) to which 1.5 mM Ca^{++} was added. Cells were then placed in buffer depleted of calcium and kept on ice. Neutrophils were suspended at physiologic concentrations (5×10^6–10^7/ml) in 37°C buffer and turbulently stirred with a small magnet (500 rpm) in cytometry test tubes (12 × 75 mm; Falcon Tubes; Becton, Dickinson, & Co., Lincoln Park, NJ; sample volume 0.5 ml). Optimum neutrophil aggregation was produced within a range of stir speeds between 400 and 700 rpm, which were calibrated using a stroboscope on the stir apparatus. The best reproducibility of kinetic particle data was obtained at 500 rpm. Lower stir speeds failed to produce high enough encounter frequencies between the cells to attain significant aggregation. Stir speeds above 700 rpm produced shear stresses large enough to prevent attachment as well as rip apart formed aggregates.

Aggregation Measurements

Cells were incubated for 2 min in buffer with Ca^{++} (1.5 mM), stained with LDS-751 (Exciton Chemical Company Inc., Dayton, OH) as described below and then aggregation was stimulated with 100 or 1,000 nM formyl hexapeptide (Bachem BioScience Inc., Philadelphia, PA). LDS-751 is a vital nucleic acid stain that homogeneously stains cells and allows detection of aggregates that exhibit integral multiples of the singlet fluorescence channel number (Terstappen et al., 1988). This dye is excited at 488 nm and has a peak emission at 670 nm. LDS-751 at a concentration of 0.2 μg/ml was added at 20 μl/10^7 cells. The cell suspensions were then incubated at 37°C for 2–3 min. Uptake of LDS-751 was found to be rapid at 37°C with a half-time of ~30 s and a stable fluorescence signal by 2 min. At 4°C the uptake was much slower and the staining heterogeneous.

Monoclonal antibody IB4 to the CD18 subunit of CR3 was provided by Dr. K. Arfors (Pharmacia Experimental Medicine, La Jolla, CA). Fab fragments were prepared and labeled with fluorescein isothiocyanate (Molecular Probes Inc., Eugene, OR). The formyl peptide antagonist (t-boc-phe-leu-phe-leu-phe) was obtained from Vega Biotechnologies, Inc. (Tucson, AZ). Formyl peptide binding to its receptor on neutrophils was inhibited by addition of 200-fold excess t-boc (2×10^{-5} M), which binds to the formyl peptide receptor.

Detection of Neutrophil Aggregation

Aggregate formation after stimulation was measured both in real time on live cells and in fixed cell samples. A FACScan (a registered trademark of Becton Dickinson Immunocytometry Systems, San Jose, CA) flow cytometer was used for the analysis of cellular and subcellular events. For fixed cell measurements, 100-μl aliquots of cell suspension were fixed in 3% formalin in Hepes buffer. Real-time analysis of aggregation was quantitated using four parameters on the cytometer: autofluorescence (FL2), side scatter (SSC), and forward light scatter (FSC), and LDS-751 fluorescence (FL3). In fixed cells, F-actin staining was achieved using *N*-(7-nitrobenz-2-oxa-1,3-diazol-4-yl)-phallacidin (Molecular Probes Inc.) as previously described (Sklar et al., 1985) and detected as FL1. Data was analyzed from dotplots of fluorescence intensity on the horizontal axis and SSC on the vertical axis (see Fig. 1 and 2). Quantitation was based on the histograms where the fluorescence of individual particle populations increases linearly with particle size. Each measurement contained between 3,000 and 5,000 particles. The parameters were stored in list mode and analyzed using FACScan research software (a registered trademark of Becton Dickinson Immunocytometry Systems).

Binding of IB4 to Cells and Its Effect on Cell Function

Cells were incubated with FITC-IB4-Fab at a saturating concentration of 5 μg/ml at 4°C for 30 min. The number of antibody molecules bound per cell was computed as follows. (*a*) The FL1 detection setting on the FACScan was calibrated in terms of the mean fluorescence channel number per known number of equivalent soluble fluorescein molecules which are bound to calibration beads (Flow Cytometry Standards Corporation, Research Triangle, NC). (*b*) The average fluorescent intensity per labeled antibody molecule (F/P ratio) was measured using Simply Cellular beads (Flow Cytometry Standards Corporation), which contain a known number of binding sites for IgG per bead. (*c*) The mean channel number of FITC-IB4-Fab bound to neutrophils was quantitated. (*d*) By dividing the equivalent soluble fluoresceins per cell from the cytometer calibration curve by the effective *F/P* ratio, the number of antibody molecules bound per cell was obtained.

Continuous measurements of the kinetics of IB4 binding in cell suspension was performed using the same approach as described previously for binding of fluorescent peptides to cell surface receptors (Sklar et al., 1985). We pointed out previously that flow cytometry intrinsically discriminates free and bound fluorescent ligand and that the background fluorescence can be obtained by preincubating cells with excess unlabeled ligand (in this case 100-fold excess IB4). Specific binding was obtained by subtracting the total IB4 channel number from the background fluorescence. To achieve rapid

equilibration of IB4 in stimulated cell suspension, IB4 was added at a saturating concentration of 10 μg/ml, after formyl peptide stimulated aggregation. The particle distribution of the stimulated neutrophils was observed on FL3 as the LDS-751 fluorescence. The content of IB4 on singlet and doublet populations obtained from mean channel values of specific binding was compared with values obtained in the same populations using the LDS-751 mean channels of singlets and doublets. The number of IB4 sites within the contact region of doublets was estimated from the fluorescence ratio of doublets to singlets at concentrations of 0.2–10 μg/ml of IB4. The number of sites was then computed as $(2\text{-}D/S)^*S$, where 2 represents the ratio of staining of doublets to singlets for LDS-751, D/S represents the ratio of the mean channels for IB4 staining of doublets to singlets, and S is the estimated number of sites on a singlet.

The Aggregation Model

The model is intended to account for the kinetics of aggregate formation and dissolution. The model is based on the geometry of each aggregate species and uniform aggregation and disaggregation rates. Several simplifying assumptions are implicit in the formalism. Particles are proposed to interact as a function of the product of their concentration and relative surface area (e.g., a doublet is twice as reactive as a singlet) and thus aggregates should form with roughly equal probability for cell attachment to any given site. Since triplets and higher order aggregates can form complex shapes, the number of aggregates in a given geometry should be proportional to the available surface area. By limiting the cell concentrations, the contributions of quartets and larger aggregates are small so complex geometries are essentially negligible in the calculations. In the case of triplets, a small fraction of the aggregates are predicted to be "triangular," accounting for no more than a few percent of the cell population. Mass is conserved for the system such that the total number of cells making up the aggregates is constant with time. The cell concentrations are defined in units of P (1 physiological unit = 5×10^6 cells/ml).

Four rate parameters define the aggregation of resting and stimulated cells. These parameters are denoted as: k^r_{agg} = aggregation rate constant, resting cells; k^s_{agg} = aggregation rate constant, stimulated cells; k^r_{disagg} = disaggregation rate constant, resting cells; k^s_{disagg} = disaggregation rate constant, stimulated cells. The units for both the resting (k^r_{agg}) and stimulated aggregation rates (k^s_{agg}) are 1/P/min. The units for the disaggregation rates (k^r_{disagg} and k^s_{disagg}) are 1/min. The particle formation geometries are indicated schematically as shown below.

	Particles		Geometry
	S + S	$\underset{k_{disagg}}{\overset{k_{agg}}{\rightleftharpoons}}$	(Doublet)
or			
	S + D	$\rightleftharpoons$	(Triplet)
or			
	D + D S + T	$\rightleftharpoons$	(Quartet)
or			
	S + Qa T + D	$\rightleftharpoons$	(Pentuplet)

Five differential equations describe a first order, linear approximation of the time rate of change of each aggregate species. The data for the model are the initial particle concentrations and the aggregation and disaggregation rates. The coefficients that accompany each particle species arise from a statistical analysis based on the aggregate geometries and the assumptions of the model as provided above. They represent the product of the number of available geometries and the fractional areas available for particle attachment. An example for the generation of the coefficients for quartets is shown in Table I.

$$dS/dt = k^s_{disagg}\,(33/48\,Pe + 7/9\,Qa + T + 2D) - k^s_{agg}\,(S)\,(2S + 2D + 3T + 4Qa) \quad (1)$$

$$dD/dt = k^s_{disagg}\,(15/48\,Pe + 4/9\,Qa + T - D) + k^s_{agg}\,((S)^2 - (D)\,(2S + 8D + 6T)) \quad (2)$$

$$dT/dt = k^s_{disagg}\,(15/48\,Pe + 7/9\,Qa - T) + k^s_{agg}\,(2(S)\,(D) - (T)\,(3S + 6D)) \quad (3)$$

$$dQa/dt = k^s_{disagg}\,(33/48\,Pe - Qa) + k^s_{agg}\,((3T)\,(S) + (2D)^2 - (4Qa)\,(S)) \quad (4)$$

$$dPe/dt = k^s_{agg}\,((6T)\,(D) + (4Qa)\,(S)) - k^s_{disagg}\,(Pe) \quad (5)$$

The rate constants are obtained by experiment as described below. The five differential equations are numerically integrated using an iterative Euler method to solve for the concentration of each aggregate species over time. The linear model may also be adapted to include nonlinear effects such as multiple binding sites between particles, or formation of much larger aggregates. However, at physiological cell concentrations aggregates larger than pentuplets formed by multiple binding sites are not detected.

Results

Cytometric Detection of Aggregates

Neutrophil aggregates ranging from singlets to pentuplets were resolved in real time and for fixed aliquots of cells in suspension on the FACScan flow cytometer. Dotplots of right-angle light scatter plotted against the LDS-751 fluorescence emission are presented in Fig. 1 for cells fixed at intervals over the time course of stimulated aggregation (*a*), and cells measured in real time (*b*). Quantitation of the particle population for each aggregate species was obtained using analysis gates on the histograms of LDS-751 fluorescence shown above each dotplot. LDS-751 mean channel values of nonsinglets were integral multiples of the singlet values. Resolution of each aggregated species was comparable for the fixed and live cell preparations.

After the 2-min incubation with LDS-751 there were >98% singlets and few larger aggregates. Stimulation with 1 μM formyl hexapeptide was followed, within 10 s, by the formation of doublets and larger aggregates. On live cells, analysis required 10–15 s for measurement of ~5,000 particles. A time interval of ~5 s was required for data storage and reset of the acquisition function of the computer. The nonsinglet populations reached a maximum between 45 s and 1 min after stimulation with formyl peptide. It was confirmed that these aggregates represented all of the nonsinglet population as detected on the FL3-SSC dotplot window. At the time point of maximum aggregation the total particle concentration typically decreased by 15–20%. This was accompanied by a similar decrease in the FACScan particle detection rate and increase in the time for acquisition of a fixed number of particle events (see Table III). After 120 s the large particles began to disaggregate. By 300 s the disaggregation phase was complete with few doublets and triplets still remaining.

Quantitation of the particle distribution for the same cell sample as measured on the FACScan in fixed and live cell suspensions is compared in Table II. A high cell density of 5×10^7 cells/ml was stimulated with hexapeptide and measured in real time on the FACScan while aliquots were taken and fixed for subsequent cytometric quantitation. At the point of maximum aggregation the live and fixed particle distributions varied by <12% for any particle size.

To test the reliability of LDS-751 fluorescent intensity in resolving the aggregate populations, a multiparameter analysis was carried out. Shown in Fig. 2 are dot plots of cells fixed at the time point of maximum aggregation. Particles exhibiting mean channel values up to fivefold greater than singlets (i.e., pentuplets) were resolved and quantitated by gating each particle size on the histograms shown above the dotplots. Results are provided in Table III. Side scatter vs. forward light scatter measurement for 10^7/ml cells are presented in Fig. 2 *a*. Side scatter increases proportionally with particle size. Forward scatter also increased for nonsin-

Table I. Probability Coefficients of Each Particle Species for the Time Rate of Change of Quartets in Eq. 4

	Disaggregation				Aggregation			
	Geometry				Geometry			
	Initial	Final	Fraction	Number of sites to form Qa	Probability coefficient (±)	Initial	Final	Fraction	Sites to form Qa	Probability coefficient (±)
S			1					1	1	+1
D			1					1	2	+2
T			1					1	3	+3
				2/3						
Qa*			2/3		6/9			2/3	4/4	
				1/3	−1					−4
			1/3	3/3	3/9			1/3	4/4	
Pe			1/3	1/2	1/6					
			7/12	1/2	14/48					
					+33/48					
			1/12	4/4	4/48					

The particle geometries for aggregation and disaggregation and the fraction of each configuration are shown. The product of the geometry fraction with the number of sites that form quartets (Qa) yields the probability coefficient of quartet formation (+), or breakup (−) for each particle species. (Qa*: As an example linear and nonlinear Qa are estimated to reflect 2/3 and 1/3 of the population respectively. If a single cell–cell contact is broken, the linear aggregate break is 2/3 into S+T and 1/3 into D+D. Nonlinear aggregates, which make up 1/3 of the population, break up always into S+T. The resulting disaggregation coefficient for this population of Qa is −1.) A similar analysis is employed to generate the probability coefficient for Pe which contain 3 nonlinear particle configurations each of which forms Qa by breaking a single cell–cell contact. Pe also disaggregate into smaller particles which accounts for the probability coefficient being <1. Since S, D, and T cannot disaggregate to form Qa there is no probability coefficient. Aggregation of S, D, and T yields Qa as a function of the number of sites for formation. Qa always combine with S to form Pe, therefore depleting their population.

glets but there was a large range and poor resolution. F-actin content per particle was measured on FL1 and plotted against side scatter in Fig. 2 *b*. The resolution was comparable and there was virtually no difference between analyses based on LDS-751 or F-actin content over the entire particle distribution. Cell autofluorescence as measured at a wavelength of 585 nm on FL2 was also used to distinguish singlets and larger aggregates. This parameter is sensitive to particle size

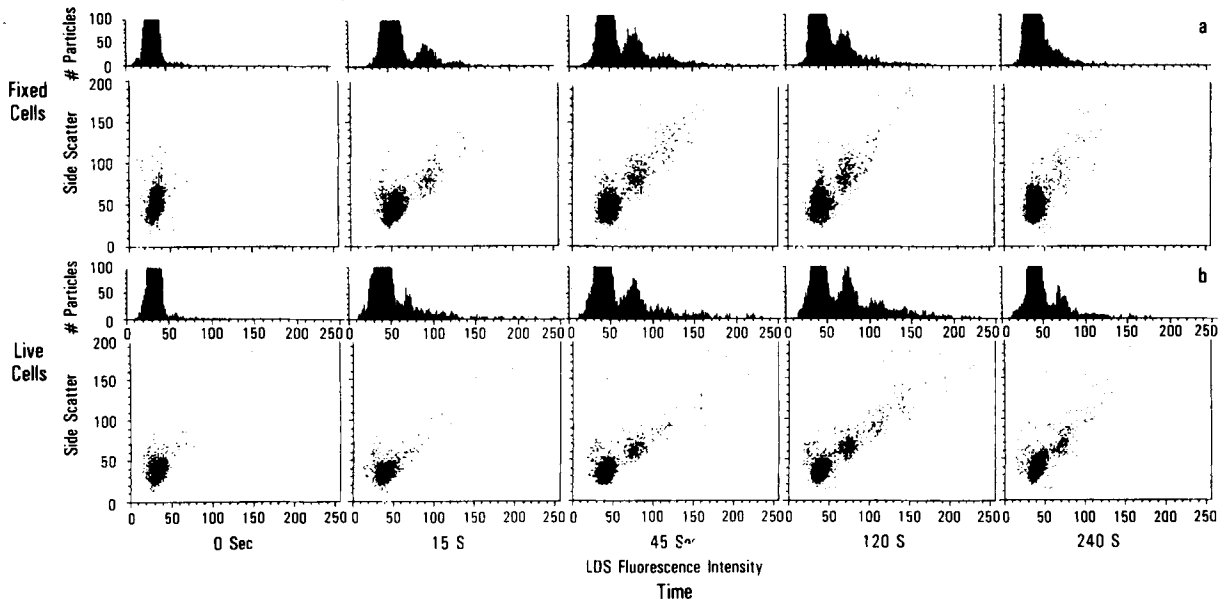

Figure 1. Time course of neutrophil aggregation for (*a*) fixed cells and (*b*) live cell suspensions at a concentration of 10^7 cells/ml. Cells were incubated at 37°C with LDS-751 (0.2 μg/ml) and then stimulated with formyl peptide (1 μM) at $t = 0$ s. Analysis of particle size distribution as performed on a Becton-Dickinson FACScan cytometer. Dot plots of side scatter plotted vs. LDS-751 fluorescence intensity (at 670 nm, FL3) were used to generate histograms as shown above each dot plot. Quantitation of the particle size distribution was performed with analysis gates on particles ranging from singlets to pentuplets.

Table II. Fixed and Live Cell LDS-751 Analysis as Measured on the FACScan

Particles	Fixed	Live
	%	%
S	53.3	57.1
D	24.7	21.5
T	14.6	13.6
Qa	7.4	8.1

Cells at a concentration of 5 × 10^7/ml were stimulated with 1 μM formyl hexapeptide. Analysis was performed at the time of maximal aggregation.

and density (e.g., the intracellular granule content) and increases (shifts to the right) during the stimulation timecourse. Resolution of the particle distribution using cell autofluorescence was found to be most useful for fixed cell samples. A 2% difference was found between autofluorescence and LDS-751 fluorescent detection of the number of nonsinglets. The best resolution of particle distribution was obtained with LDS-751 fluorescence in which particles up to pentuplets could be resolved (Fig. 2 *d*). It should be noted that cell staining with LDS-751 does not interfere with the extent or time course of aggregation as confirmed by comparable aggregation as measured by F-actin content in the absence of LDS-751.

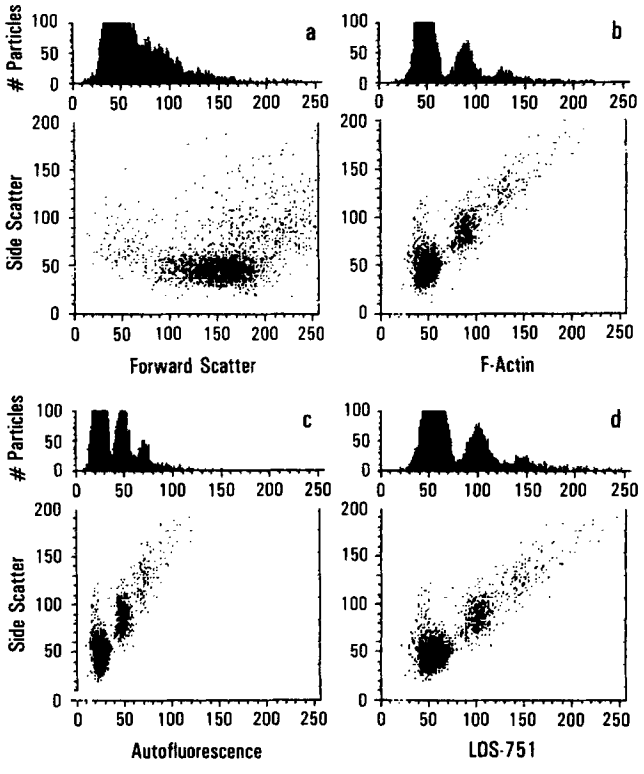

Figure 2. Multiparameter analysis of particle distribution at maximum aggregation (t = 40 s) for neutrophils (2 × 10^7 cells/ml) stimulated with formylated hexapeptide (1 μM). Dot plots of side scatter plotted with the following parameters: (*a*) forward light scatter; (*b*) F-actin content; (*c*) cell autofluorescence (at 585 nm, FL2); (*d*) LDS-751 fluorescence. Particle distributions were derived from analysis gates on the histograms shown above each parameter. The percent total of each particle species is provided in Table III.

Table III. Multiparameter Analysis of Particle Detection As Measured on the FACScan

Particle	F-Actin	AutoFL.	SSC	LDS-751
S	76.5	76.6	75.6	76.2
D	17.1	16.8	18.7	17.2
T	5.1	5.2	4.2	5.0
Qa	1.0	1.2	1.2	1.1
Pe	0.3	0.3	0.4	0.6

Cells at a concentration of 2 × 10^7/ml were stimulated with 1 μM formyl hexapeptide and the analysis performed on fixed cells at the time point of maximum aggregation. Data have units of percent particles. It was confirmed that larger aggregates did not go undetected since the particle detection rate (pdr) varied in parallel with the calculated change in particle concentration (pc) between maximum aggregation and disaggregation time points. pc = 14% ± 17; pdr = 13% ± 12; n = 10.

Extraction of Quantitative Aggregation Information

The time course of neutrophil aggregation as defined in Fig. 1 shows a stage of aggregate formation between 0 and 45 s, a plateau phase in which aggregates remain at fairly constant levels between 45 and 120 s, and a disaggregation phase beyond 120 s. To characterize the particle behavior, it is necessary to define rate constants in both stimulated and resting cells.

Resting Cells. The approach to defining aggregation constants is to examine the extent and time course of aggregate formation as a function of cell concentration and cell stimulation. Two approaches to characterize resting behavior were used. In the first approach, the concentration dependence of aggregate formation in unstimulated cells was evaluated. In the second approach, the transition from stimulated back to resting behavior was evaluated. The extent of aggregate formation varied with cell density in resting cells (Table IV), with no more than 0.5% residual doublets even in very diluted cell suspensions. An apparent equilibrium constant when there are only singlets and doublets can be represented as:

$$Keq = [D]/[S][S] = k^r_{agg}/k^r_{disagg} \quad (6)$$

The apparent equilibrium constant at the highest cell concentration was no greater than ~0.005. When corrected for residual nondisaggregating doublets (i.e., 0.4% doublets at 10^6 cells/ml), the average Keq ~ 0.004.

An estimate of the rate of disaggregation in resting cells was obtained by examining disaggregation after the transition from activated to resting cells. We have previously shown that cells treated with formyl peptide (1 μM) returned to the inactivated state when receptor occupancy was blocked with an antagonist (Sklar et al., 1985). In these experiments, the turnoff kinetics were reported to involve a

Table IV. Apparent Equilibrium Constants

Cell concentration	S	D	Keq (1/P)
10^8	92.8	6.0	0.004
2 × 10^7	97.4	2.5	0.007
10^7	98.7	1.1	0.005
10^6	99.5	0.4	0.02

Keq was computed from Eq. 6 over a 100-fold change in cell concentration. The 0.4% doublets observed at 10^6 cells/ml apparently represent residual aggregates which do not disaggregate.

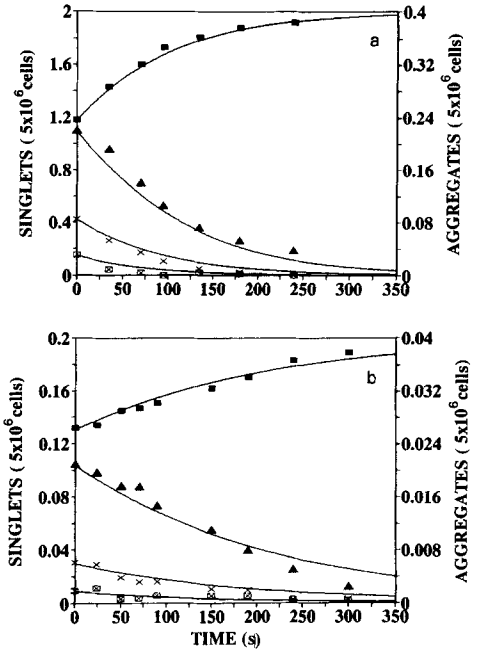

Figure 3. Kinetics of particle disaggregation as measured on the cytometer based on FL3 (LDS-751 fluorescence). Cells (10^7/ml) were stimulated (formyl hexapeptide 1 μM) and brought to maximum aggregation before treatment with (*a*) t-boc-phe-leu-phe-leu-phe (60 μM) or (*b*) 1:100 dilution into buffer containing stimulus (formyl hexapeptide, 1 μM). The particle kinetics of singlets (■), doublets (▲), triplets (×), and quartets (□) was modeled with the aggregation component eliminated (maximum aggregation at t = 0) and the results shown as solid lines.

period of 30 s during which cell activation signals decayed followed by accelerated disaggregation. As shown in Fig. 3 *a*, we present the behavior of formyl peptide stimulated cells 30 s after they were treated with the antagonist. An estimate for the unstimulated k^r_{disagg} was obtained by fitting the linear model to the particle data with a value of 1.1 ± 0.2/min. Since the disaggregation is limited by the transition from stimulated to resting cells, this estimate for k^r_{disagg} should be viewed as a lower limit to the disaggregation rate constant of resting cells. Taken together and interpreted according to Eq. 6, the equilibrium observations on resting cells and the apparent disaggregation rates as cells return to their inactive forms imply that the rate of aggregation in resting cells is no more than 0.005/min, meaning that <1% of the cells at physiological concentrations will stick together each minute.

Disaggregation Rates in Stimulated Cells. Disaggregation rate constants were obtained by isolating disaggregation behavior from aggregation behavior under conditions where net aggregation was limited. We studied the disaggregation of already stimulated and aggregated cells that were then diluted into buffer containing stimulus so that they remain activated. The stimulated disaggregation rate was computed by fitting the particle data with the model assuming a net aggregation rate which had been effectively reduced to 0 due to the dilution of the cells. A representative dilution experiment is shown in Fig. 3 *b*. It is seen that stimulated cells can remain well attached for at least 180 s after dilution before the disaggregation rate becomes characteristic of nonstimulated cells. Before this increase in the disaggregation rate, cells that had been diluted from a density of 10^8/ml to 10^6/ml at the point of maximum aggregate formation, yielded an average value for the apparent stimulated k^s_{disagg} of 0.38 ± 0.1/min (n = 24). Since there may be loss of cell activation contributing to disaggregation, the rate obtained in the dilution protocol should be viewed as an upper limit.

Aggregation Rates in Stimulated Cells. Previous studies have shown that singlet cells are activated in a relatively uniform fashion, based on the formation of F-actin when stimulated with an optimal dose of formyl peptide. Estimates of k^s_{agg} can be obtained by fitting aggregation kinetics assuming uniform aggregation behavior with the model and using measured disaggregation rates. Stimulated aggregation rate constants were obtained by fitting the initial rate data after stimulation with the empirically measured k^s_{disagg} as shown in Fig. 4. The aggregation kinetics were investigated as a function of cell concentration from 5 × 10^6 to 2 × 10^7 cells/ml.

Within 10 s of the addition of stimulus neutrophil aggregation was detected. The first phase of aggregation typically lasted from 20–60 s and required the largest stimulated aggregation rate (k^s_{agg} = 0.15 ± 0.15 /P/min, n = 16). For a fourfold increase of cell concentration the k^s_{agg} for the first phase was approximately constant, typically varying <50%. All cell concentrations show biphasic aggregation kinetics in which the stimulated time course was fit in two phases with

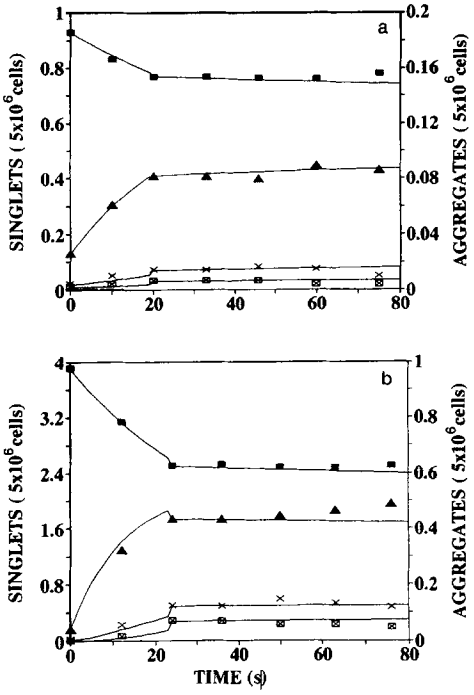

Figure 4. Particle distribution as measured on the cytometer after stimulation of (*a*) 5 × 10^6 cells/ml and (*b*) 2 × 10^7 cells/ml with formyl hexapeptide (1 μM). The number of particles measured as singlets (■), doublets (▲), triplets (×), and quartets (□) was quantitated using LDS-751 fluorescence. Solid lines depict the results of the linear model of aggregation for the first two phases of aggregation with rates. (*a*) Phase I, 0–25 s, k^s_{agg} = 0.3/P/min, k^s_{disagg} = 0.2/min. Phase II, 25–80 s, k^s_{agg} = 0.05/P/min, k^s_{disagg} = 0.2/min. (*b*) Phase I, 0–20 s, k^s_{agg} = 0.15/P/min, k^s_{disagg} = 0.2/min. Phase II, 20–80 s, k^s_{agg} = 0.02/P/min, k^s_{disagg} = 0.2/min.

Table V. Aggregation and Disaggregation Rates Over the Three Phases

Phase	Aggregation rate (1/P/min)	Disaggregation rate (1/min)
I	s 0.15 ± 0.5	s $\leqslant 0.38 \pm 0.1$
II	s→r $\leqslant 0.05$	s $\leqslant 0.38 \pm 0.1$
III	r $\leqslant 0.005$	s→r $\geqslant 1.1 \pm 0.2$

Aggregation and disaggregation rates within the aggregation phase (I), plateau phase (II), and disaggregation phase (III). Values given as means or upper limits obtained from modeling 16 experiments. Stimulated state denoted by *s*, resting state denoted by *r*.

distinct aggregation rates as discussed below. A second phase of the time course in which new aggregate formation reached a plateau lasted from 30–200 s. In the plateau phase data was fit with an aggregation rate typical of resting cells (Table V).

Models of Aggregation and Disaggregation. Kinetic data on the formation of singlets, doublets, triplets, and quartets was obtained at ~10-s intervals over the entire time course of stimulated aggregation (Fig. 5). Three phases with distinct aggregation and disaggregation rates were used to model the kinetic particle data. The entire time course could be accounted for using the resting and stimulated disaggregation rates whose derivation is described above. The first phase lasted 50 s and was fit to the data with k^s_{agg} = 0.15/P/min, k^s_{disagg} = 0.2/min. It appears that a rapid transition of the aggregation rate from the resting to stimulated value is the predominant factor in modeling the particle kinetics of the first phase. As long as the stimulated disaggregation rate was small (≪1/min) modeling the k^s_{agg} was relatively insensitive to changes of k^s_{disagg} in this phase.

After the first phase of the time course, formation of nonsinglets reached a plateau in which the data could be fit with a resting aggregation rate (≪0.15/P/min) and a stimulated disaggregation rate (<0.4/min). This analysis was confirmed by measuring the disaggregation rate constant in both the aggregation and plateau phases. We observed that upon dilution into buffer with stimulus the disaggregation rates in either phase were within 10% and ≪1.

In the third phase of the time course disaggregation predominated. The data are consistent with a large increase in the rate of disaggregation to the resting cell level (>1/min), and an aggregation rate also typical of that in resting cells (<0.01/P/min).

Mechanism of Aggregation Probed with IB4. In principle the particle kinetics in the second phase could be fit with a variety of aggregation rates and disaggregation rates. To validate our interpretation of the second phase in which new aggregates are limited, we used IB4 to characterize the adhesive sites available in the aggregates. We also examined the impact of IB4 on aggregation behavior. A more detailed characterization of the behavior of the epitope for IB4 will be reported elsewhere (Chambers, J. D., S. I. Simon, and L. A. Sklar, manuscript in preparation). We have confirmed that preincubation of cells with saturating concentrations of FITC-IB4-Fab (2.5 μg/ml for 30 min at 4°C) blocks aggregation of formyl peptide stimulated cells. The initial concentration of 98% singlets changes little throughout the stimulatory timecourse. At saturation there are ~200,000 CD18 sites on the neutrophil which upregulate by no more than ~10%/min after stimulation.

In the untreated cell sample (Fig. 6 *a*), the control aggregation time course had an initial aggregation phase that lasted 60 s and a plateau phase that lasted ~2.5 min. These phases were fit with typical rates. For simplicity only singlets and doublets are shown in the aggregation time courses. To investigate aggregate stability during the plateau, aggregates were diluted after 40 s 1:10 into buffer containing stimulus (Fig. 6 *b*). After dilution, the aggregates exhibit kinetics qualitatively similar to that of the control, but have a slightly increased rate of disaggregation and an earlier onset of resting behavior than the control of Fig. 6 *a*. In contrast, IB4 (10 μg/ml) added just after maximum aggregation, had a profound effect on the particle kinetics (Fig. 6 *c*). A rapid breakup to a portion of the aggregates occurred immediately after antibody addition. Moreover, the plateau phase in which the number of aggregates remained fairly constant lasted only 30 s, this was 2 min shorter than that of the control.

The kinetics of IB4 binding to sites on singlets and doublets in this experiment are presented in Fig. 6 *d*. The IB4-Fab binds to CD18 such that available sites on the cells are 90% occupied within the first 30 s of IB4 addition to the stimulated cell suspension. (The binding rate constant is 3.4 × 10^5/M/s; after binding, adhesive sites remained occupied over the aggregation time course since the IB4 dissociation rate is 2.5 × 10^{-3}/s; Chambers, J. D., S. I. Simon, and L. A. Sklar, manuscript in preparation). The ratio of the number of IB4-Fab binding sites on doublets and singlets was between 1.7 and 1.8, compared to the LDS-751 doublet to singlet fluorescence channel ratio of ~2.0. We estimate that at IB4 equilibrium ($t \sim 100$ s, Fig. 6 *d*), there are in the doublets no more than 10–15% or between 65,000 and 97,000 sites in the contact region which were inaccessible to antibody binding compared to the number of sites available on the singlets.

At 70 s when IB4 was 90% bound to singlets and doublets, there was a transition from the plateau to an enhanced dis-

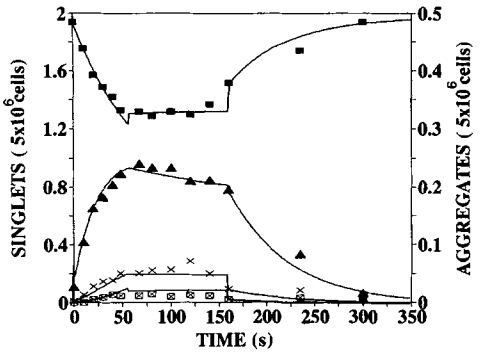

Figure 5. Particle distribution over the complete time course of aggregation. Neutrophils (10^7 cells/ml) were stimulated with formyl hexapeptide (1 μM) and the particle kinetics are plotted for singlets to quartets. The linear model was split into three phases to predict the reversible time course of aggregation (*solid lines*). The rate constants for the three phases were as follows. Phase I, 0–48 s, k^s_{agg} = 0.15/P/min, k^s_{disagg} = 0.2/min. Phase II, 48–140 s, k^s_{agg} = 0.02/P/min, k^s_{disagg} = 0.2/min. Phase III, 140–350 s, k^s_{agg} = 0.01/P/min, k^s_{disagg} = 1.2/min.

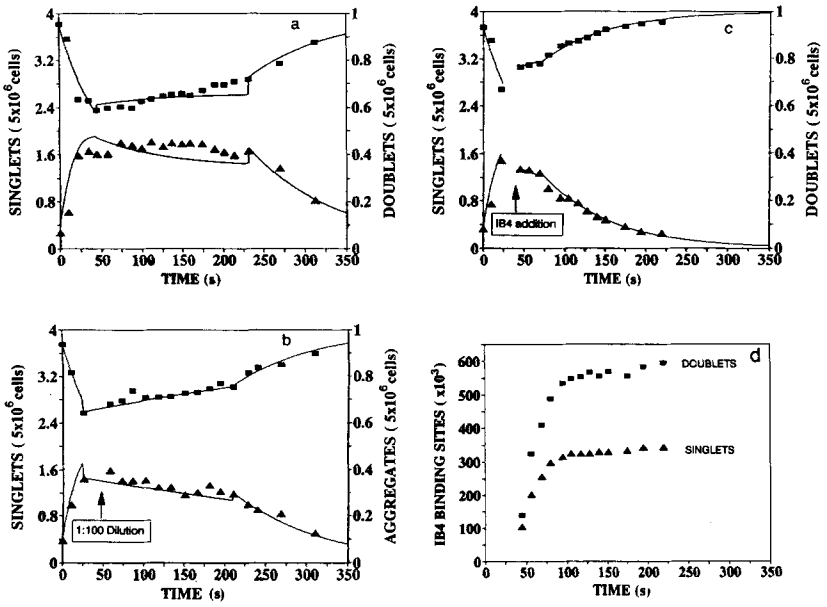

Figure 6. Comparison of the effect of cell dilution and IB4 on particle distribution kinetics. (*a*) The time course of formyl peptide stimulated neutrophil (2×10^7 cells/ml) aggregation. Particle kinetics for singlets (■) and doublets (▲) were modeled in three phases. Solid lines with rates. Phase I, 0–45 s, k^s_{agg} = 0.12/P/min, k^s_{disagg} = 0.2/min. Phase II, 45–232 s, k^s_{agg} = 0.02/P/min, k^s_{disagg} = 0.2/min. Phase III, 232–350 s, k^s_{agg} = 0.005/P/min, k^s_{disagg} = 0.8/min. (*b*) Neutrophils that have been stimulated to maximum aggregation and then diluted 1:10 in buffer with stimulus at 40 s. Particle kinetics were modeled in three phases. Solid line with rates. Phase I, 0–25 s, k^s_{agg} = 0.13/P/min, k^s_{disagg} = 0.2/min. Phase II, 25–210 s, k^s_{agg} = 0/P/min, k^s_{disagg} = 0.4/min. Phase III, 210–350 s, k^s_{agg} = 0/P/min, k^s_{disagg} = 0.9/min. (*c*) FITC-IB4-Fab was added (10 μg/ml at 35 s) to neutrophils that were stimulated to maximum aggregation. Particle kinetics were modeled in three phases. Solid line with rates. Phase I, 0–22 s: k^s_{agg} = 0.1/P/min, k^s_{disagg} = 0.2/min. Phase II, 22–69 s: k^s_{agg} = 0/P/min k^s_{disagg} = 0.2/min. Phase III, 69–350 s: k^s_{agg} = 0/P/min, k^s_{disagg} = 0.9/min. Particle kinetics modeled in phases II and III neglected the aggregation components due to intervention which abrogated the aggregation behavior. (*d*) Binding kinetics of FITC-IB4-Fab to the surface of formyl peptide stimulated neutrophils after addition of 10 μg/ml at t = 35 s. The mean channel number for specifically bound FITC-IB4-Fab to singlets (▲) and doublets (■) is shown. Channel numbers were converted to the number of sites using Simply Cellular Standards.

aggregation phase. An interpretation of the impact of the molecular manipulation on the macroscopic aggregation behavior is required. An argument will be developed in the Discussion that individual adhesive bonds are breaking and forming in the contact region during cell–cell contact.

Discussion

Kinetic Analysis of Aggregation

Neutrophils in a well-stirred suspension stimulated with formyl peptide undergo reversible aggregation. A method by which the kinetics of aggregate formation is measured on the flow cytometer both on live cells and on fixed cells is described. Kinetics of formyl peptide stimulated aggregation in real time was achieved with a temporal resolution of 5–10 s between sequential cytometric measurements. Particles ranging from singlets to pentuplets were resolved and quantitated by LDS-751 fluorescence. LDS-751 is a vital nucleic acid stain in which fluorescence intensity increases linearly with aggregate size. A multiparameter analysis that compared particle discrimination using F-actin content, side scatter, cell autofluorescence, and LDS-751 fluorescence yielded less than a 2% difference between parameters in determining aggregate distribution. LDS-751 quantitation of aggregation as measured in real time on live cells and compared with cell samples fixed over the same stimulation time course showed less than a 12% difference. These latter results indicate that the live aggregates are stable in the hydrodynamics of the flow cytometer.

Models of Aggregation Kinetics

A linear model, with independent measurements of rate processes for stimulated and nonstimulated cells succeeded in fitting the distribution of singlet through pentuplets over the complex time course of stimulated aggregation and disaggregation. The primary assumption in the model is that the efficiency of adherence is proportional to particle surface area. Models without this assumption do not in our hands adequately describe the data. Further geometrical constraints taking into account complex shapes represent refinements to the model which typically reflect a small percentage of the total cell mass of the system. Models in which nonlinear effects such as cell attachment to multiple sites on an aggregate can be formulated. Since the fraction of particles containing three or more cells is usually <7%, the higher order computation based on a nonlinear model would vary from the linear model by no more than 1–2%. These nonlinear considerations are nonetheless realistic for analysis of aggregation at high cell concentration or for enhanced aggregation.

Three distinct phases were used to model formyl peptide stimulated neutrophil aggregation (Table V). Formation of nonsinglets proceeded rapidly within 10 s after stimulation and the kinetic data was fit with the largest k^s_{agg}. A transition of the k^s_{agg} was evident entering the second phase of aggregation which required a rate at least three to fourfold less than that of the initial fast phase. Stimulated rates of disaggregation did not change significantly between the first two phases as confirmed by measuring k^s_{disagg} after cell dilution within each phase. In the third phase disaggregation predominated for the final 2–3 min of the time course. A transition from the stimulated to the unstimulated disaggregation rate was characterized by an increase of the k_{disagg} of four to fivefold from the stimulated disaggregation rate.

Analysis of Aggregation Within Each Phase

Several other cell responses that occur rapidly after formyl

peptide stimulation are F-actin formation (Sklar et al., 1985) and cell surface ruffling (Hoffstein et al., 1982). The fast kinetics of particle formation during the first phase may be in part driven by a change in cell shape and surface projections. The fact that the encounter frequency increases as the third power of the cell radius supports this notion (Karino and Goldsmith, 1979).

Based on the cell dilution experiments, it appears that the aggregates that have formed by the end of the first phase remain intact during the second phase. Thus a relatively static equilibrium exists between the singlets and aggregates rather than one in which new aggregates are continually forming and breaking. Since the intravascular encounter frequency for leukocytes can be as high as 14/cell/min in postcapillary venules (Schmid-Schoenbein et al., 1987), the transition from a stimulated to a resting rate of aggregation at the end of the first stimulatory phase may function to limit the formation of large leukoemboli. The time frame of maximum aggregate formation by the end of the first phase (~30–60 s) is comparable to the formyl peptide induced phosphorylation profile of CD18 which peaks at 30 s and is completely reversed by 5 min (Chatilla et al., 1989).

When cell stimulation was arrested with the antagonist to the formyl peptide receptor, the aggregatory response decayed after a transient of ~30 s to reveal the nonstimulated disaggregation rate. This also is consistent with the behavior of several other cell responses such as actin polymerization, Ca^{++} elevation, and cell surface ruffling (Sklar et al., 1985). These responses were found to be elicited by relatively low levels of receptor occupancy (<1,000 receptors/cell) but required the binding of a majority of the stimulatory receptors to sustain the response.

Cell Encounter Frequency and Hydrodynamics

Cells interacting in suspension as a result of the rotation of a magnetic stir bar undergo collisions which may be described in terms of the encounter frequency. A model that estimates the encounter frequency for a suspension of platelets interacting in a simple shear flow (Karino and Goldsmith, 1979) was applied to neutrophils mixing in suspension. Extending the analogy to a density of 5×10^6 cells/ml which are being stirred at 500 rpm, the theory predicts that each cell experiences approximately six collisions with adjacent cells per minute. A comparison with the resting aggregation rate (k^r_{agg} <0.005/cell/min) reveals that no more than 1 in 1,000 cells remained aggregated. After formyl peptide stimulation the aggregation rate increased to a value of 0.1–0.2/P/min suggesting an increase in the collision efficiency to roughly 1 in 10 cells remaining adhered.

Knowledge of the efficiency with which cell collisions result in aggregate formation permits an evaluation of the critical parameters such as the shear stress, cell concentration, or surface morphology in aggregate formation. It appeared that the stimulated aggregation rates remained approximately constant over a fourfold increase in cell concentration from 5×10^6 to 2×10^7 cells/ml. Since the encounter frequency may increase up to 16-fold for a 4-fold increase in cell concentration, the ability of the model to fit the data with rates of aggregation within a narrow range suggests the general form of the concentration dependent terms in the model are appropriate.

Shear rates which were achieved by the stir bar within the cytometry tubes at 500 rpm were estimated to be ≥30/s (Karino and Goldsmith, 1979). Since the shear field within the cytometry tube is too complex for precise determination, only order of magnitude estimates can be made. In a laminar fluid stream with the shear stress given by Stoke's law as $\tau = 6\eta G$ (with buffer viscosity $\eta = 7.5 \times 10^{-3}$ dyn/s/cm^{-2} and shear rate G as estimated), the shear stress imposed upon the cell aggregates is approximated to be ~1 dyn/cm^2. This range of values is well within that which supports neutrophil–endothelial cell adhesion (Ley et al., 1989).

Molecular Insight into Aggregation Mechanisms

We are beginning to gain insight into the molecular mechanisms of cell–cell adhesion through a macroscopic description of aggregation. Preincubation of cells with IB4-Fab at a saturating concentration (2.5 μg/ml) completely blocked formyl peptide stimulated neutrophil aggregation. These cells expressed ~200,000 sites on their surface before peptide stimulation, and upregulated ~10% per minute over the first two phases of aggregation. When FITC-IB4-Fab is added during the time course of formyl peptide stimulation at supraoptimal concentrations (10 μg/ml), 90% of the sites were bound within ~30 s after addition (Fig. 6 *d*) and aggregation ceased (Fig. 6 *c*).

From a functional standpoint, in control or diluted control samples relatively few new aggregates were formed during the 3 min of the plateau phase before the transition to disaggregation (Fig. 6, *a* and *b*). In contrast, IB4-Fab addition caused an initial breakup of what appear to be weak aggregates, similar to that seen in the dilution time course. By the time IB4 binding approached 90% saturation, cells began to disaggregate. Explaining these functional aspects requires an interpretation of the molecular activity in the contact region.

First, an estimate of sites in the contact region is possible. We note that LDS-751 doublets are two times as bright as singlets whereas IB4 doublets are ~1.75 times as bright as singlets. This result suggests that no more than 10–15% of the CD18 sites on the surface are confined to the contact region on adjacent cells where they are inaccessible to the Fab. Regardless of the quantitative interpretation, we would suggest that IB4 binds to adhesive sites as they become available within the contact region of adjacent cells. The kinetics of the enhanced disaggregation phase may therefore reflect the rate at which adhesive sites become available for binding to the IB4 Fab antibody. Since we do not know if there is a threshold value of sites for maintaining contact we hypothesize that adhesive bonds are disassembling over this time frame, a period comparable to the dephosphorylation of CD18. Under these circumstances, the average lifetime for the active CD18 population and adhesive bonds they participate in would be 30–60 s as computed from the rate of particle breakup in the disaggregation phase ($0.693/k_{disagg}$). We would hypothesize that continued occupancy of stimulatory receptors is required to sustain the existing adhesive bonds which in turn hold together the aggregates. Disaggregation ensues within 30 s of addition of formyl peptide receptor antagonist, comparable to the time lag observed for disaggregation in response to IB4 treatment.

By defining the rates at which IB4 binds to new sites within the contact region during the three phases of the aggregation time course, it should ultimately be possible to establish the

relationship between the number and duration of adhesive sites and their effect on the macroscopic rates of stimulated aggregation.

We are grateful to Dr. Karl Arfors for providing us with IB4 monoclonal antibodies and use of his laboratory resources.

Dr. Scott Simon is a Fellow of the American Heart Association, California Affiliate. This work was supported in part by United States Public Health Service grants AI19032 and HL43026 to L. A. Sklar.

Received for publication 25 April 1990 and in revised form 6 August 1990.

References

Arnout, M. A., R. M. Hakim, R. F. Todd, III, N. Dana, H. R. Colten. 1985. Increased expression of an adhesion-promoting surface glycoprotein in the granulocytopenia of hemodialysis. *N. Eng. J. Med.* 312:457–462.

Bell, G. I. 1978. Models for the specific adhesion of cells to cells. *Science (Wash. DC).* 200:618–627.

Bell, G. I. 1981. Estimate of the sticking probability for cells in uniform shear flow with adhesion caused by specific bonds. *Cell. Biophys.* 3:289–304.

Bowen, T. J., H. D. Ochs, L. C. Altman, T. H. Price, D. E. Von Epps, D. L. Brautigan, R. E. Rosin, W. D. Perkins, B. M. Babior, S. J. Klebanoff, and R. J. Wedgwood. 1982. Severe recurrent bacterial infections associated with defective adherence in a cell-associated glycoprotein. *J. Pediatr.* 101:932–938.

Capo, C., F. Garrouste, A. M. Benoleil, P. Bongrand, A. Ryder, and G. Bell. 1982. Concanavalin-A-mediated thymocyte agglutination: a model for a quantitative study of cell adhesion. *J. Cell Sci.* 56:21–48.

Chang, H. M., and C. R. Robertson. 1976. Platelet aggregation by laminar shear and Brownian motion. *Ann. Biomed. Eng.* 4:151–183.

Chatila, T. A., R. S. Geha, and M. A. Arnaout. 1989. Constitutive and stimulus-induced phosphorylation of CD11/CD18 leukocyte adhesion molecules. *J. Cell Biol.* 109:3435–3444.

Dana, N., B. Styrt, J. D. Griffin, R. F. Todd, III, M. S. Kempner, and M. A. Arnaut. 1986. Two functional domains in the phagocyte membrane glycoprotein MO identified with monoclonal antibodies. *J. Immunol.* 137:3259–3263.

Diener, A. M., P. G. Beatty, H. D. Ochs, and J. M. Harlan. 1985. The role of neutrophil membrane glycoprotein 150 (GP-150) in neutrophil mediated endothelial cell injury *in vitro*. *J. Immunol.* 135:537–543.

Hoffstein, S. T., B. S. Friedman, and G. Wiessmann. 1982. Degranulation, membrane addition, and shape change during chemotactic factor-induced aggregation of human neutrophils. *J. Cell Biol.* 95:234–241.

Jacob, H. S., and D. Hammerschmidt. 1981. Complement-induced granulocyte aggregation. Importance in myocardial infraction and shock lung. *J. Am. Med. Assoc.* 245:2013–2017.

Karino, T., and H. L. Goldsmith. 1979. Aggregation of human platelets in an annular vortex distal to a tubular expansion. *Microvasc. Res.* 17:217–237.

Klebanoff, J. S., P. G. Beatty, R. D. Schreiber, H. Ochs, and A. M. Waltersdorph. 1985. Effect of antibody directed against complement receptor on phagocytosis by polymorphonuclear leukocytes: use of iodination as a convenient measure of phagocytosis. *J. Immunol.* 134:1153–1159.

Kuypers, T. W., and D. Roos. 1989. Leukocyte membrane adhesion proteins LFA-1, CR3 and p150,95: a review of functional and regulatory aspects. *Res. Immunol.* 140:461–486.

Ley, K., E. Lundgren, E. Berger, and K. E. Arfors. 1989. Shear-dependent inhibition of granulocyte adhesion to cultured endothelium by dextran sulfate. *Blood.* 73:1324–1330.

Luscinskas, F. W., A. F. Brock, M. A. Arnaout, and M. A. Gimbrone, Jr. 1989. Endothelial-leukocyte adhesion molecule-7-dependent and leukocyte (CD11/CD18)-dependent mechanisms contribute to polymorphonuclear leukocyte adhesion to cytokine-activated human vascular endothelium. *J. Immunol.* 142:2257–2263.

Patarroyo, M., and M. W. Makgoba. 1989. Leukocyte adhesion to cells: molecular basis, physiological relevance and abnormalities. *Scand. J. Immunol.* 30:129–164.

Schmid-Schoenbein, G. W., S. I. Simon, D. R. Newcome, and R. L. Engler. 1987. Effects of AQA-39 on granulocytes in the microcirculation of rat mesentery. *Eur. Heart J. Suppl. L.* 8:75–81.

Schwartz, B. R., H. D. Ochs, P. G. Beatty, and J. M. Harlan. 1985. A monoclonal antibody-defined membrane antigen complex is required for neutrophil-neutrophil aggregation. *Blood.* 65:1553–1556.

Sklar, L. A., G. M. Omann, and R. G. Painter. 1985. Relationship of actin polymerization and depolymerization to light scattering in human neutrophils: dependence on receptor occupancy and intracellular Ca^{++}. *J. Cell Biol.* 101:1161–1166.

Terstappen, L. W. M. M., V. O. Shoh, M. P. Conrad, D. Recktenwald, and M. R. Cohen. 1988. Discriminating between damaged and intact cells in fixed flow cytometry samples. *Cytometry.* 9:477–484.

Tolley, J. O., G. M. Omann, and A. J. Jesaitis. 1987. A high yield, high purity elutriation method for preparing human granulocytes demonstrating enhanced longevity and chemoattractant induced responses. *J. Leukocyte Biol.* 42:43–50.

Yuli, I., and R. Snyderman. 1984. Rapid changes in light scattering from human polymorphonuclear leukocytes exposed to chemoattractants discrete responses correlated with chemotactic and secretory proteins. *J. Clin. Invest.* 73:1408–1417.